A Global Land Reanalysis System with the Norwegian Climate Prediction Model: NorCPM-Land

Akhilesh S. Nair[1,2], François Counillon[1,2,3], Noel Keenlyside[1,2]

[1]Geophysical Institute, University of Bergen, Bergen, Norway.

[2]Bjerknes Center for Climate Research, Bergen, Norway.

[3]Nansen Environmental and Remote Sensing Center, Bergen, Norway.

Corresponding author: Akhilesh Nair (Akhilesh.nair@uib.no)

Key Points:

- We introduce a novel strategy for the development of a stochastic system for land data assimilation.
- We evaluate the impact of enhanced soil moisture states on the land-atmosphere coupling.
- Our reanalysis system provides improved long-term estimates of land water and energy balance components.

Abstract

At continental mid-latitude, soil moisture (SM) is a key component of the climate systems and land surface initialization is crucial for subseasonal-to-seasonal (S2S) predictions. We introduce a new stochastic global land reanalysis system called the Norwegian Climate Prediction Model Land (NorCPM-Land), which will be used to initialize the land component of the Norwegian Climate Prediction Model (NorCPM). We assimilate the blended SM from the European Space Agency's Climate Change Initiative (ESA CCI) into a 30-member offline simulation of the land surface Community Land Model (CLM). Fluxes are provided by 30-member historical simulations of the full coupled NorCPM. The Ensemble Kalman Filter (EnKF) updates daily the soil column from the SM data using the cumulative density function matching method.The NorCPM-Land is currently produced for 40 years from 1980 to 2019. Assimilation significantly improves the land surface state variability and reduces error by 10.5% when validated using independent SM observations and by reanalysis estimates from ERA5-Land. It also yields an improvement of land surface energy, runoff and net primary production. We demonstrate that adjusting the underlying soil moisture considerably enhances the ability to simulate land surface state dynamics.

Plain Language Summary

Soil moisture (SM) is a key element of the climate system, and the insitial land surface condtion is important for accurate subseasonal-to-seasonal (S2S) predictions. We have developed the Norwegian Climate Prediction Model Land (NorCPM-Land), which is a new land reanalysis system providing improved land initial condition. It will be used to initialise the land part of the Norwegian Climate Prediction Model (NorCPM). We assimilate the combined SM from the Climate Change Initiative of the European Space Agency (ESA CCI) into an offline simulation of the land surface using thirty realizations of the Community Land Model (CLM). Input to the CLM are given by historical simulations of the NorCPM with all 30 members. SM data are used by the Ensemble Kalman Filter (EnKF) to update the soil column every day. This is done by matching the cumulative distribution function. The improved land condition from NorCPM-Land has been made available for the past 40 years, from 1980 to 2019. Assimilation makes a big difference in the variability of the state of the land surface and cuts error by 10.5% when validated with independent SM observations. It also leads to an improvement in land surface energy, runoff, and vegetation productivity. We show that changing the moisture of the soil makes it much easier to accurately model the state of the land surface.

1 Introduction

Subseasonal to seasonal (S2S) forecasting has substantial societal implications, especially in the water management, agribusiness, and emergency response sectors (Merryfield et al., 2020). There is, however, a considerable gap in accurate prediction at S2S range because of the chaotic processes underlying predictability sources (Meehl et al., 2021; Mariotti et al., 2018). Thus, it is essential to get better understanding of such predictability and to develop more accurate monitoring and prediction systems. It is largely accepted that the land surface is an important factor in determining the predictability and variability of the climate at S2S timescales (Koster et al. 2004; Guo et al. 2011). Regional climate can change in response to alterations in land-atmosphere feedbacks and/or surface conditions (Dirmeyer and Halder, 2016). In regions where there is substantial land-atmosphere coupling, the soil moisture (SM) exerts a direct influence on the atmosphere. The exchange of latent and sensible heat fluxes in these places changes the land-atmosphere feedbacks that are influenced by SM (Koster et al. 2004). SM has also been found to

influence hydro-meteorological factors such as temperature and precipitation (Koster et al., 2004; Seneviratne et al., 2010; Taylor et al., 2012). Previous studies have shown that SM affects the accuracy of seasonal predictions (Fischer et al., 2007; Koster et al., 2010; Dirmeyer and Halder, 2016; Dirmeyer et al., 2018; Seo et al., 2019; Seo et al., 2020). The persistence of SM anomalies over time (also known as SM memory) is stronger than that of meteorological variables, hence enhancing subseasonal forecasts (Orth and Seneviratne, 2012; McColl et al., 2017; Santanello et al., 2018). Therefore, land surface is one of the primary factors influencing S2S forecasts with a 2- to 4-week lead time (Mariotti et al., 2018). Consequently, improving the initial condition of the SM is crucial for enhancing the S2S prediction capabilities.

In this paper, we introduce a data assimilation (DA) scheme for improving the SM initialisation in the Norwegian Climate Prediction Model (NorCPM) with the long-term aim to improve S2S predictions. NorCPM is based on the Norwegian Earth System Model version 1 (NorESM1) and the Ensemble Kalman Filter (EnKF; Evensen, 2003) to provide climate reanalyses (Counillon et al., 2016) and seasonal-to-decadal climate predictions (Counillon et al., 2014, Bethke et al. 2021). The present version of NorCPM uses a closely coupled DA framework to update the states of the ocean and sea ice components (Penny et al. 2017). However, the current version of NorCPM does not update the states of the atmosphere and the land components in the DA phase. Here we build a reanalysis product to improve the NorCPM's land initialization but preserving the model climatology so that hindcast drift are minimized.

This study relies on the offline community land model (CLM) in NorESM to develop the new Norwegian Land Reanalysis System (NorCPM-Land). To simulate the main land surface processes, the CLM leverages water and energy balance equations (Oleson et al., 2013). Among the several land surface state variables, SM plays a vital role in regulating the exchange of water and energy between the land and atmosphere. The development of the planetary boundary layer and near-surface atmospheric fluxes are known to be affected by fluctuations in SM (Santanello et al., 2011). The prevailing SM state is characterized by a large degree of temporal and spatial variability. This is because it is profoundly affected by a wide range of factors, including precipitation, land cover, and soil texture. The CLM provides spatially and temporally continuous estimates of SM at a range of soil depths down to the water table at configurable resolutions. CLM simulation skills, on the other hand, are susceptible to uncertainty because of bias in atmospheric forcing and the inability of model physics to replicate accurate land surface processes. SM observations are frequently obtained using sparse in situ networks or satellite remote sensing, and their spatiotemporal coverage is thus limited. One of the most severe constraints is that the currently available remote sensing can only offer measurements of the surface SM. To circumvent these constraints, satellite SM measurements are integrated synergistically with a land surface model (LSM) using the DA method (Reichle and Koster, 2004; Drush et al., 2009; de Rosnay et al., 2013; Kumar et al., 2012; Nair and Indu, 2016; Nair and Indu, 2019; Nair et al., 2020). The DA method delivers improved land initial states for prediction models in several applications, including S2S forecasting. Assimilation of satellite SM estimate enhances the ability to forecast surface humidity, air temperature, geopotential height, and precipitation (Zheng et al., 2018).

Satellite remote sensing in the microwave range of the electromagnetic spectrum, especially in the L-band (1-2 GHz) and C-band (4-8 GHz), is ideal for SM monitoring (Carver et al., 1985). At low frequencies (1-5 GHz), the sharp difference in dielectric constant between dry soil (approximately 3) and water (approximately 80) underpins ability of microwave remote sensing to capture SM (Ulaby et al., 1996). With increasing frequency, the sensitivity of the

dielectric constant to SM diminishes (Hallikainen et al., 1985). Low-frequency microwave channels are also known for having less vegetation interference. A variety of satellite-borne sensors working in the passive and active microwave areas have provided near-surface SM products. Unlike passive microwave sensors, which estimate SM from the surface emitted brightness temperature, active microwave sensors offer near-surface SM at global scales by detecting the backscattered value from the surface. Some of the widely used satellite SM products stems from Advanced Scatterometer (ASCAT) aboard Meteorological Operational (METOP) satellites (Wagner et al., 2013), multi-frequency polarimetric microwave radiometer WindSat aboard Coriolis satellite (Gaiser et al., 2004), Advanced Microwave Scanning Radiometer Earth Observing System (AMSR-E; Njoku et al., 2003) aboard Aqua satellite, Advanced Microwave Scanning Radiometer 2 (AMSR2; Imaoka et al., 2010) aboard the Global Change Observation Mission-Water (GCOM-W) satellite, the recent satellites in L band from the Soil Moisture Ocean Salinity (SMOS) mission (Kerr et al., 2010) and the Soil Moisture Active Passive (SMAP) mission (Entekhabi et al., 2010). The availability of these satellite missions has paved the way for different SM products from individual satellites as well as blended multi-satellite products such as the European Space Agency's Climate Change Initiative (ESA CCI). The offline assimilation system developed in this study is designed to incorporate daily SM data from the ESA CCI into the CLM using the EnKF method. In the following sections, we describe in detail the assimilation strategy utilized in this study and the assessment standards used.

2 Land Reanalysis with the Norwegian Climate Prediction Model (NorCPM-Land)

The NorCPM-Land provides daily estimates of different land surface state variables pertaining to water and energy balance, globally at a spatial resolution of 1.9° × 2.5° of the model and by assimilating SM data from ESA-CCI. Although direct assimilation of SM data into NorCPM would be ideal, the system is currently only working with offline assimilation - meaning that the model is stopped, the state written on disk, data assimilation applied on the files and the model restarted. The time required for initializing the model and writing the input/output is burdensome (see, e.g., Karspeck et al. 2018), and the required daily frequency for SM data assimilation is not feasible with our current configuration. Therefore, we produce a land reanalysis from the offline land component forced with atmospheric fluxes from an ensemble of historical runs of NorESM (the ESM used in NorCPM) and by assimilating daily SM data. As such the reanalysis and the model used for running the prediction are the same. This will prevent numerical shocks that can emerge when the initial state is taken from a different model system.

2.1 Norwegian Earth System Model

This study employs NorESM1-ME (Bentsen et al., 2013; Tjiputra et al., 2013). NorESM1 is based on the Community Earth System Model version 1.0.3 (CESM1; Hurrell et al., 2012), with difference in the ocean component, atmospheric chemistry, and ocean biogeochemistry. The ocean component in NorESM is an updated version of the isopycnal coordinate ocean model MICOM (Bleck et al., 1992). The new model (referred to as Bergen Layered Ocean Model) includes implementation of an incremental remapping for isopycnal advection, calculation of pressure gradient force by correct vertical integration of in-situ density, changed parameterization of isopycnal and diapycnal mixing processes, and a novel split-mixed layer formulation (Bentsen et al., 2013). It uses 51 isopycnal layers and two layers for representing the bulk mixed layer with time-evolving thicknesses and densities. The ocean biogeochemistry is based on the Hamburg

Ocean Carbon Cycle Model (HAMOCC, Assmann et al., 2010; Tjiputra et al., 2012). The sea ice component is a version of the Los Alamos Sea ice model (CICE4, Gent et al. 2011; Holland et al. 2012). The ocean and the sea-ice model have a horizontal resolution of approximately 1°. The atmosphere component is a version of the Community Atmosphere Model (CAM4-Oslo, Kirkevåg et al. 2013), which provides choices for aerosol and cloud chemistry (Kirkevåg et al., 2013). CAM4 has a horizontal resolution of 1.9° latitude and 2.5° longitude and 26 vertical levels in a hybrid sigma-pressure coordinate; CLM4 follows the same horizontal grid as CAM4. CLM4 is described in more details in the next section.

2.2 Community Land Model

The CLM 4.0 coupled in the NorESM is used in this work to develop an offline assimilation system. The CLM model is an integrated land model that is based on water and energy balance equations. Land surface in CLM 4.0 follows a subgrid hierarchy, with each grid cell consisting of land units, columns, and plant functional types (PFTs). Grid cells can have different numbers of land units, like lakes, glaciers, vegetation, and urban areas. Each column in the vegetated land units has 15 layers of soil and 5 layers of snow, depending on the snow depth. The soil profile in CLM 4.5 consists of 15 strata with depths ranging from 7.100635 mm, 27.925 mm, 62.25858 mm, 118.8651 mm, 212.1934 mm, 366.0658 mm, 619.7585 mm, 1038.027 mm, 1727.635 mm, 2864.607 mm, 4739.157 mm, 7829.766 mm, 12925.32 mm in each active grid cell. The top 10 hydrologically active strata are used to compute the soil moisture. To simulate changes in canopy water, surface water, snow water, soil water, soil ice, and water in the unconfined aquifer, the model parameterizes interception, throughfall, canopy drip, snow accumulation and melt, water transfer between snow layers, infiltration, evaporation, surface runoff, sub-surface drainage, redistribution within the soil column, and groundwater discharge and recharge. In CLM the multilayer vertical moisture and energy transfer in a one-dimensional soil model are predicted using a modified Richard's equation. Similarly, to derive the land surface fluxes, the similarity theory developed by Monin and Obukhov is adopted. CLM4.5 considers the spatial heterogeneity of the land surface, and it simulates the soil moisture, soil temperature, infiltration, evapotranspiration, sensible heat flux, latent heat flux, and soil heat flux (Oleson et al., 2013). The soil hydraulic and thermal characteristics in CLM4.5 are derived from the pedotransfer functions of sand and clay (Cosby et al., 1984) and organic properties of the soil (Lawrence and Slater, 2007). In this work, the CLM is configured by incorporating following components: DATM; CLM; SICE; SOCN; RTM; SGLC; SWAV. The resolution of the model is set to f19_g16 globally, with a total of 288 (longitude) 192 (latitude) grid cells.

2.3 Data Assimilation using Ensemble Square Root Filter

Data assimilation system in this study is built on the Ensemble Kalman Filter (EnKF) approach, which implies that observations are related to the true model state ($\mathbf{x^{True}}$).

$$\mathbf{y} = \mathbf{H}\mathbf{x}^{\mathbf{True}} + \boldsymbol{\varepsilon} \qquad \ldots\ldots (1)$$

The linear operator $\mathbf{H}$ converts the model space to observations space, where $\mathbf{y}$ is the observation vector, $\boldsymbol{\varepsilon}$ is assumed to be a Gaussian random error with zero mean and observation error covariance matrix $\mathbf{R}$. Similarly, the prediction for $\mathbf{x}$ at time with mean $\mathbf{x^f}$ is also assumed to

193 be an unbiased Gaussian error with error covariance matrix $\mathbf{P^f}$. In accordance with these postulates,
194 the ensemble mean can be updated as follows.

195 $$\mathbf{x^a} = \mathbf{x^f} + \mathbf{K}(\mathbf{y} - \mathbf{H}\mathbf{x^f}) \quad \text{..... (2)}$$

196

197 where $\mathbf{K}$ is called as Kalman gain matrix computed as in Eqn. 3

198 $$\mathbf{K} = \mathbf{P^f}\,\mathbf{H^T}\left(\mathbf{H}\mathbf{P^f}\,\mathbf{H^T} + \mathbf{R}\right)^{-1} \quad \text{..... (3)}$$

199 The superscript f and a denotes the prior (forecast or background) and the analysis
200 (posterior) estimates.

201 We use the Ensemble Square Root Filter (EnSRF) to sequentially solve the analysis without
202 the need to perturb observation values, which performs more optimally than the stochastic EnKF
203 (Whitaker and Hamill 2002). The ensemble anomalies are computed as follows:

204 $$\mathbf{x'^a} = \mathbf{x'^f} + \boldsymbol{\alpha}\mathbf{K}\left(-\mathbf{H}\mathbf{x'^f}\right) \quad \text{..... (4)}$$

205 Where $\mathbf{x'^a}$ represents the ensemble anomaly, $\mathbf{x'^f}$ indicates forecast ensemble anomaly and,

206 $\boldsymbol{\alpha} = \left(\mathbf{1} + \sqrt{\frac{\mathbf{R}}{\mathbf{H}\mathbf{P^f}\mathbf{H^T}+\mathbf{R}}}\right)^{-1}$.

207 The term $\mathbf{P^f}\mathbf{H^T}$ in Eqn. 3 is the cross-covariance computed from the ensemble between the
208 observation and the state variables updated by assimilation.

209 **2.4 Satellite Soil Moisture Estimates**

210 The ESA CCI SM v 06.1 incorporates over four decades of scatterometer-based active and
211 radiometer-based passive microwave sensors from several satellite platforms. Datasets based on
212 active sensors stems from the C-band (5.3 GHz) Active Microwave Instrument Wind
213 Scatterometer (AMI-WS ERS-1/2 SCAT, 1991–2006; AMI-WS ERS-2, 1997–2007), Advanced
214 Scatterometer (ASCAT), MetOp-A (2007–19), and MetOp–B (2012–19). While the passive
215 sensors used to generate SM are from the C-band (6.6 GHz) Scanning Multichannel Microwave
216 Radiometer (SMMR, 1979–87), the K-band (19.3 GHz) Special Sensor Microwave Imager
217 (SSM/I, 1987–2013), the X-band (10.7 GHz) Tropical Rainfall Measuring Mission (TRMM)
218 Microwave Imager (TMI, 1998–2015), the X-band (10.7 GHz) FengYun-3B Microwave Radiation
219 Imager (FY-3B/MWRI, 2011-19), and the X-band (10.7 GHz) Global Precipitation Measurement
220 (GPM, 2014–20). The Advanced Microwave Scanning Radiometer 2 (AMSR-2, 20012–19),
221 WindSat (2007–12), and the Advanced Microwave Scanning Radiometer for Earth Observing
222 System (AMSR-E, 2002–11) are three more passive platforms that measure in the X band and C
223 band. The Soil Moisture Active and Passive mission (SMAP, 2015–19) and Soil Moisture and
224 Ocean Salinity (SMOS, 2010-19) are the other two passive sensors that measure in the L band (1.4
225 GHz). The ESA CCI SM algorithm combines and harmonizes these many active and passive
226 satellite SM retrievals to provide a consistently intercalibrated and quality-controlled SM product

with a wider spatial and temporal coverage than any single-sensor SM products. The combined dataset, which combines both active and passive products, spans 41 years (1979–2020), has a geographical resolution of 0.25°, a temporal resolution of 1 day, and a perceived soil thickness of 5 cm, although it does have data gaps where and when there are no measurements.

2.5 Workflow and practical implementation

The NorCPM-Land processing phase can be broken down into two distinct stages. In stage 1, the ensemble of atmospheric forcing required to run the offline CLM simulation is generated using historical runs of NorESM for the period 1980 to 2019 at a temporal resolution of 3 hours. In stage 2, soil moisture from ESA CCI is assimilated daily into the offline CLM. Figure 1 shows the flowchart of NorCPM-Land processing steps.

In stage 1, the fully coupled NorESM generates precipitation, air temperature, humidity, pressure, and radiation forcing components at 3 hourly intervals that are needed to run offline CLM. The 30 member ensemble historical simulations are produced by selecting random initial conditions from a stable preindustrial simulation and integrating the ensemble from 1850 to 2019 using CMIP5 historical forcings and there after the RCP8.5 is used (Taylor et al. 2012).

In stage 2, daily surface SM is assimilated daily to update CLM soil profile. The ensemble forecast, $\mathbf{x}_t^f$ consists of the 30-model snapshot of SM from NorESM. The SM observations from ESA CCI are used to update the model SM using Eqn. (4) and (2). Only the first ten layers of the 15 that comprise the CLM state are updated, while the other variables of the state vector remain intact (e.g. temperature). We update every vertical profile independently. Assimilation of SM occurs solely on land units defined by vegetation. We do not incorporate densely vegetated regions, however, due to the uncertainty in SM estimations from the ESA CCI over thick canopy cover. In addition, we exclusively update the liquid SM in soil profiles, so avoiding erroneous updates in ice SM, which are challenging to estimate by microwave remote sensing (Ulaby et al., 1992). This implies that we do not assimilate SM in the presence of snow or frozen SM. There is a very strong mismatch between SM observations from ESA CCI and the corresponding model estimates. This is handled by using cumulative distribution function (CDF) mapping (Reichle and Koster, 2004; Kumar et al., 2012). The CDF mapping is done for each calendar month and for each grid point. The CDF is computed from the daily values of the calendar month over the 40 years of the observations and from the daily output of the ensemble mean of the 30 member offline

CLM run without assimilation. Finally, we use a small multiplicative inflation (Anderson 2001) of 1.05 to prevent a collapse of the ensemble spread.

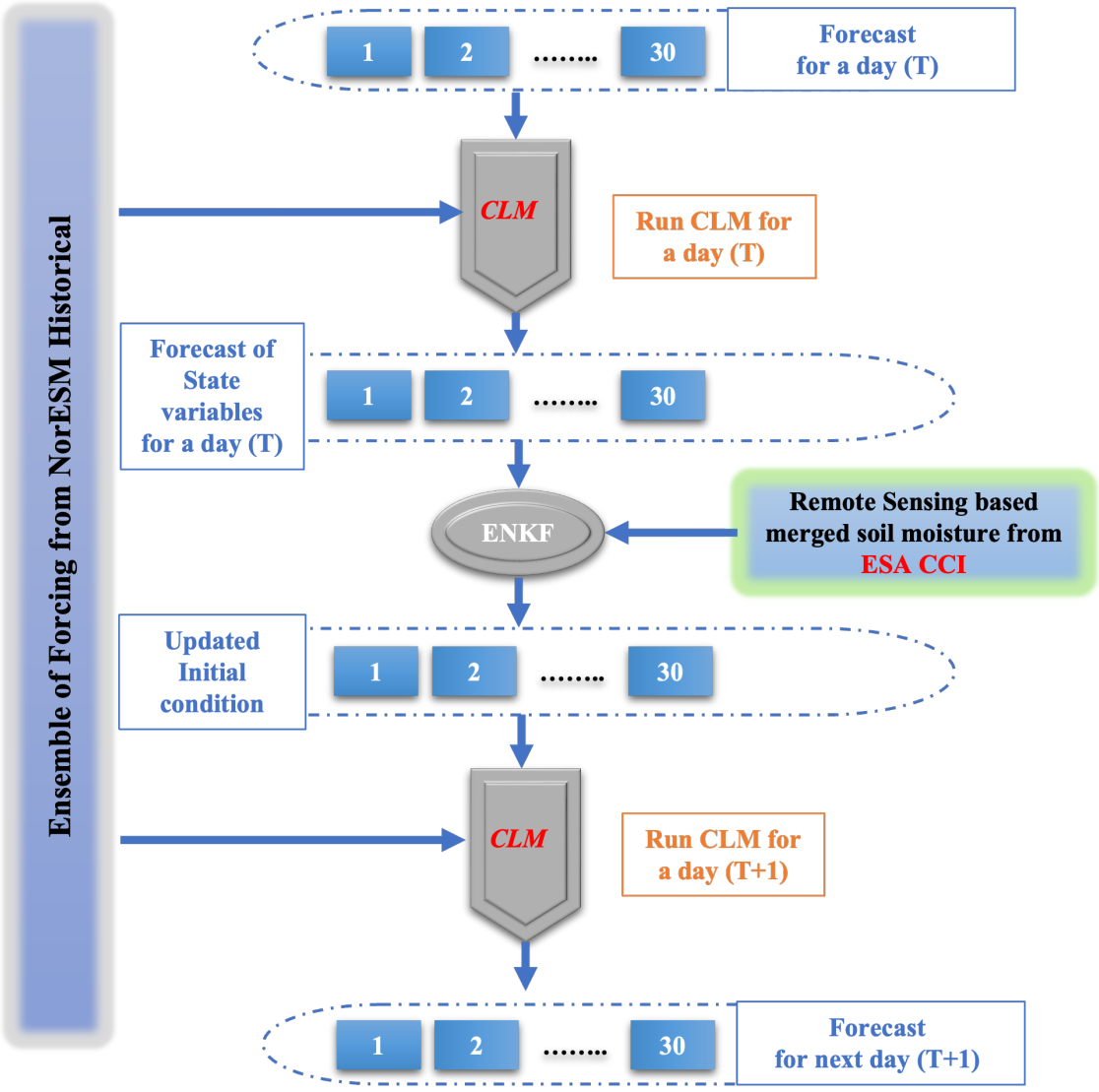

Figure 1. Flowchart of NorCPM-Land

3 Validation data sets

3.1 In Situ Soil Moisture Measurement

This study utilizes in situ soil moisture observations from the International SM Network for continental domain validation (ISMN; Dorigo et al. 2011) as primary source of SM validation. We concentrate on three locations with rather dense observational coverage. Over the CONUS, the Atmospheric Radiation Measurement (ARM), the FLUXNET–AMERIFLUX, the Cosmic-Ray Soil Moisture Observing System (COSMOS; Zreda et al. 2012), the Plate Boundary Observatory (PBO H2O; Larson et al. 2008), the Soil Climate Analysis Network (SCAN; Schaefer et al. 2007), the Snowpack Telemetry (SNOTEL). For validation over Europe, the FR_Aqui (Al-Yaari et al.

2018), Danish Hydrological Observatory and Exploratorium (HOBE; Jensen and Refsgaard 2018), ORACLE, REMEDHUS (González-Zamora et al. 2019), the Norwegian water resources and energy directorate (NVE), the Finnish network (FMI; Ikonen et al., 2018). For validation over Asia, the central Tibetan Plateau (CTP_SMTMN; Yang et al., 2013), MAQU (Dente et al., 2012) networks are used. This study further includes only hourly readings to a depth of 5 centimeters that are classified as "excellent quality" and concurrently measured for validation purposes. After filtering the hourly data, the daily mean soil moisture is calculated, and only locations with more than thirty percent of the validation date range are used for validation.

3.2 ERA5-Land

One of the independent data sources used to validate our reanalysis is the ECMWF ERA5-land reanalysis. The new ERA5-Land reanalysis was generated by forcing offline LSM with the ERA5 (Hersbach et al. 2020) data. Because the atmospheric analysis of ERA5 is forcing this product, the assimilated data indirectly impact simulations. The system does not assimilate SM observations explicitly. The Copernicus Climate Change Service provides it with the same temporal resolution as ERA5 (hourly resolution), but with a higher spatial resolution of 0.1°x0.1°. The primary properties of this product were outlined in Müloz-Sabater et al. (2021), and it is now accessible from 1950 to the present at https://cds.climate.copernicus.eu. ERA5-Land is built around the ECMWF land surface model: the Carbon Hydrology-Tiled ECMWF Scheme for Surface Exchanges over Land (HTESSEL). Under the HTESSEL system, each land grid-box is subdivided into up to six fractions (tiles) (bare ground, low and high vegetation, intercepted water, shaded and exposed snow). Each fraction has features that define distinct heat and water fluxes utilized to solve an energy balance equation for the tile skin temperature. According to Müloz-Sabater et al. (2021), ERA5-Land considers grids with more than 50% of their area covered by glaciers to be glacier grids, assuming a constant snow depth of 10 m.

The ERA5-Land is forced by ERA5, which is produced from data assimilations and dynamic models, and integrates observations into globally comprehensive fields. ERA5 assimilates additional observations and input data, which enhances the observed changes in climatic forcing compared to the preceding product (ERA-Interim) and at a higher temporal and horizontal resolution. The average number of observations absorbed by ERA5 has risen from around 0.75 million per day in 1979 to nearly 24 million per day by the end of 2018. The observation operators, which convert model values to observation equivalents, and the processing of observations in the forecast system have been vastly improved in ERA5 compared to ERA-Interim. Instead of the RTTOV-7 operator used in ERA-Interim, it employs RTTOV-11 as the observation operator for radiance data. Additionally, it assimilates several humidity-sensitive satellite channels utilizing the all-sky technique as opposed to the clear-sky strategy used by ERA-Interim. This resolves an issue with an older assimilation method of radiances under rainy circumstances that resulted in anomalous precipitation in ERA-Interim across the entire ocean in the 1990s, in addition to offering new information in overcast and precipitating locations. ERA5 used multiple reprocessed satellite datasets gathered from space organizations and institutions in Europe, the United States, and Japan. These include atmospheric motion vector winds; ozone, radio occultation, and altimetry data; scatterometer soil moisture and wind data; and the SSMI record of satellite data sensitive to humidity over the ocean. In general, ERA5 has used many more observations than ERA-Interim, which cannot include data from the most recent satellite sensors, such as hyperspectral data from IASI and CrIS or ground-based radar data. ERA5 used around 24

million observations per day at the end of 2018, almost five times as many as ERA-Interim. ERA5 relies on 4D-Var (Courtier et al., 1994) for upper air and near surface components, an optimum interpolation (OI) approach for ocean-wave and a Land Data Assimilation System (LDAS) (de Rosnay et al., 2013). The LDAS relies on a 2D-OI for the analysis of 2m temperature and relative humidity, as well as for snow depth and density, a simplified extended Kalman filter (de Rosnay et al., 2013) for soil layers and 1D-OI for soil, ice and snow temperatures respectively.

3.3 GLDAS

The third independent validation data used in this study stems from the Global Land Data Assimilation System (GLDAS) (Rodell et al., 2004) from NASA. GLDAS is an uncoupled land data assimilation system, that drives different offline LSMs. The GLDAS currently drives five different LSMs, namely Noah (Chen et al., 1996), the Community Land Model (CLM; Dai et al., 2003), the Variable Infiltration Capacity Model (VIC; Liang et al., 1994), Mosaic (Koster and Suarez, 1992), and the Catchment land surface model (CLSM; Koster et al., 2000). GLDAS version 1 (GLDAS-1) relies on the atmospheric analysis fields from the Global Data Assimilation System (GDAS) of NCEP, the NOAA Climate Prediction Center's Merged Analysis of Precipitation (CMAP) pentad dataset, and observation-based downward shortwave and longwave radiation fields derived from the AGRicultural METeorological modeling system (AGRMET). The LSMs are forced with this combination forcing (Rodell et al., 2004). In GLDAS version 2 (GLDAS-2), two different forcing data are used, one is driven by Princeton meteorological forcing data (Sheffield et al., 2006), while the other is driven by a mixture of model and observation-based forcing datasets as utilized in GLDAS-1. In GLDAS-2 CMAP precipitation is replaced with a field from the Global Precipitation Climatology Project (GPCP), it also employs a better disaggregation method, and applies quality control to the AGRMET dataset. GLDAS-2 has three subcomponents: GLDAS-2.0, GLDAS-2.1, and GLDAS-2.2. GLDAS-2.0 is forced only with Princeton meteorological forcing and delivers a continuous record from 1948 to 2014. GLDAS-2.1 is forced by combined model and observation-based data from 2000 to the present. The GLDAS-2.0 and GLDAS-2.1 products do not assimilate any observations while, the GLDAS-2.2 products assimilate observations like surface temperature, snow cover, and Total Water Storage (TWS). There are many distinct GLDAS-2.2 products, each of which has its own unique selection of forcing data, as well as DA observation source, variable, and scheme. We use GLDAS-2.1 with CLSM as the LSM to evaluate NorCPM-land results along with ERA5-Land. It should be noted that even in GLDAS there is no explicit assimilation of SM observations. We utilise ERA5-Land and GLDAS as reference datasets to evaluate NorCPM-Land improvements because independent global in-situ SM measurements are sparse and not uniformly distributed.

3.4 Surface Runoff Data

Freshwater resources are extremely important to society, and understanding their variability is critical to water management in the context of climate change. To evaluate surface runoff, this study uses the global gridded monthly reconstruction of runoff (GRUN) from 1980 to 2014. This data was generated by leveraging in-situ streamflow measurements to train a machine learning algorithm that forecasts monthly runoff rates based on antecedent precipitation and temperature from an atmospheric reanalysis. Cross-validation is used to check the correctness of this reconstruction, which is then compared to an independent set of discharge data for major river basins. This dataset agrees with streamflow measurements on average better than an ensemble of

13 state-of-the-art global hydrological model runoff simulations (Ghiggi et al., 2019). The reconstruction's temporal span provides an unparalleled perspective of large-scale runoff variability characteristics in places with low data coverage, making it a suitable independent dataset for large-scale hydro-climatic process investigations and validation. The GRUN dataset can be found online at https://doi.org/10.6084/m9.figshare.9228176.

3.5 Net Primary Productivity

The biogeophysical processes that CLM4 simulates include the interactions of solar and longwave radiation with vegetation and soil, momentum and turbulent fluxes from vegetation and soil, heat transfer in soil and snow, hydrology of vegetation and soil, and stomatal physiology in addition to photosynthesis. The carbon-nitrogen (CN) cycle model in CLM4 simulates how carbon and nitrogen are bio-geochemically arranged in plant, litter, and soil-organic matter (Thornton et al., 2007). Plants convert carbon dioxide in the air into oxygen while producing their own sustenance. Thus, plants give the energy and oxygen that most living forms on Earth require. Plant productivity also contributes significantly to the global carbon cycle by absorbing part of the CO_2 emitted when people consume coal, oil, and other fossil fuels. Carbon that plants consume forms a part of their leaves, roots, stalks, or tree trunks, and, eventually, the soil. The net primary productivity (NPP) is the difference between the amount of carbon dioxide vegetation absorbs during photosynthesis and the amount of carbon dioxide plants emit during respiration. A negative score indicates that breakdown or respiration exceeded carbon absorption; the plants expelled more carbon into the atmosphere than they absorbed. The improvement in SM states will be propagated into the carbon cycle and enhance NPP estimations since SM is a crucial factor in plant productivity. In this study we utilize NPP estimates from Moderate Resolution Imaging Spectroradiometer (MODIS) on board Terra satellite to validate our reanalysis results. The monthly NPP data from MODIS (MOD17A3) is used as reference in this study. These datasets are available at a spatial resolution of 1km from https://lpdaac.usgs.gov/data_access/. It contains estimates of gross primary productivity (GPP), NPP and net direct quality control (NP_QC). Previous studies have reported outstanding performance of MOD17A3 NPP dataset with the observations at the global or country scale (Turner et a., 2006; Shim et al., 2014).

4 Metrics for skill assessment of NorCPM-Land

The skill of SM assimilation is evaluated by comparing reanalysis estimates with the assimilated ESA CCI SM product and with other independent measurements (as discussed in section 3). The improvement in NorCPM-Land is quantified by comparing it with performance of 30-member ensemble of offline CLM run with same initial conditions and meteorological forcing as NorCPM-Land (hereafter referred to as FREE). The ensemble-mean and reference datasets are used to calculate the performance indices. The performance indices used in this study are the Root Mean Square Error (RMSE), the anomaly correlation coefficient (ACC). Because amplitude of the seasonal changes is large and predictable, computing correlation based on estimated SM and reference data may yield misleadingly high values on the usefulness of a prediction system. As a

result, it is common practice to subtract the seasonal cycle from both datasets to validate the estimated (FREE and NorCPM-Land) and reference (ERA5-Land) before computing the ACC

$$\mathbf{RMSE} = \left[\frac{\mathbf{1}}{\mathbf{n}}\sum_{\mathbf{i=1}}^{\mathbf{n}}(\mathbf{X_i} - \mathbf{Y_i})^{\mathbf{2}}\right]^{\frac{\mathbf{1}}{\mathbf{2}}} \quad \text{..... (5)}$$

$$\mathbf{ACC} = \frac{\sum_{\mathbf{i=1}}^{\mathbf{n}}(\mathbf{X_i}-\overline{\mathbf{X}})(\mathbf{Y_i}-\overline{\mathbf{Y}})}{\sqrt{\sum_{\mathbf{i=1}}^{\mathbf{n}}(\mathbf{X_i}-\overline{\mathbf{X}})^{\mathbf{2}}\sum_{\mathbf{i=1}}^{\mathbf{n}}(\mathbf{Y_i}-\overline{\mathbf{Y}})^{\mathbf{2}}}} \quad \text{..... (6)}$$

For validation we use daily as well as monthly model state estimates. Therefore, n represents the number of estimates during the 40 years study period from 1980 to 2019. $\mathbf{X_i}$ and $\mathbf{Y_i}$ are the daily or monthly land surface state estimates (NorCPM-Land, FREE) and independent reference observations, respectively. $\overline{\mathbf{X}}$, $\overline{\mathbf{Y}}$ are the monthly mean of land surface state estimates and independent reference observations respectively. It should be noted that in this study, the ACC is calculated using monthly values. The improvement in NorCPM-land skill after DA is represented using the reduction of RMSE (RRMSE).

$$\boldsymbol{RRMSE} = \frac{\boldsymbol{RMSE_{FREE} - RMSE_{NorCPM-Land}}}{\boldsymbol{RMSE_{FREE}}} \quad \text{..... (7)}$$

We also investigate the reliability of NorCPM-Land. The reliability is evaluated by examining the spatial and temporal collocation of the total DA uncertainty with the RMSE (Counillon et al., 2016; Rodwell et al., 2016). The RMSE is calculated in this case against imperfect observations with an error variance ($\boldsymbol{\sigma_o^2}$), and the overall error is the sum of the observation and model uncertainty ($\boldsymbol{\sigma_m^2}$). The standard deviation of the model ensemble state serves as a measure for model uncertainty.

$$\boldsymbol{Total\ Error} = \sqrt{\boldsymbol{\sigma_o^2 + \sigma_m^2}} \quad \text{..... (8)}$$

The reliability of ensemble system is evaluated by dividing RMSE by the total error (hereafter referred to as reliability index). The reliability index provides a quantitative comparison of ensemble spread with respect to its predictive skill. A reliability index of one implies that the spread is ideal (Fortin et al., 2014), whereas a value more than one suggests a narrow spread (under dispersive), and a value less than one indicates a wide ensemble (over dispersive).

Because the primary purpose of this reanalysis approach is to improve S2S prediction capabilities in NorCPM, it is critical to assess the influence of SM assimilation on terrestrial atmospheric coupling. We demonstrate this using the atmospheric coupling index (ACI) (Müller et al., 2021). This index shows whether alterations to a surface flux variable can or cannot affect precipitation changes. The areas where the coupling between the land and the atmosphere is strongest are known as the land-atmosphere hot spots. The ACI is computed using latent heat flux ($\boldsymbol{\lambda E}$), and precipitation ($\boldsymbol{P}$) as in Eqn. 9.

$$\boldsymbol{ACI} = \frac{\boldsymbol{cov(\lambda E, P)}}{\boldsymbol{\sigma(\lambda E)}}, \quad \text{..... (9)}$$

where $\boldsymbol{cov(\lambda E, P)}$ represents covariance between latent heat flux and precipitation, while $\boldsymbol{\sigma(\lambda E)}$ represents the standard deviation along the time space. Areas where latent heat fluxes have

an impact on precipitation are highlighted by this indicator. This completes the full cycle of land-atmosphere coupling and is a potent sign of the direct feedback from the atmosphere to the land. The reference ACI is calculated using ERA5-Land precipitation and latent heat flux.

5 Results

5.1 Verification against assimilated SM

The accuracy of NorCPM-Land in monitoring the variability of SM is evaluated using root mean square error (RMSE) with respect to assimilated observations (i.e., the CDF match ESA-CCI), and the results are compared to the FREE run. Because the evaluation is performed using the exact same assimilated ESA CCI SM data, it is anticipated that NorCPM-Land will demonstrate a lower level of error than FREE (sanity check).

The RMSE in a perfectly reliable system equals the total error. Figure 2a shows the RMSE of FREE with respect to assimilated ESA CCI SM. Error in FREE is large because internal variability is not constrained. Similarly, Figure 2b indicates the total error in the system as defined in Eqn 8. The reduction of RMSE (RRMSE, Eqn. 7) in NorCPM-Land from FREE is shown in Figure 2c. There is a prominent reduction in RMSE throughout the domain as expected.

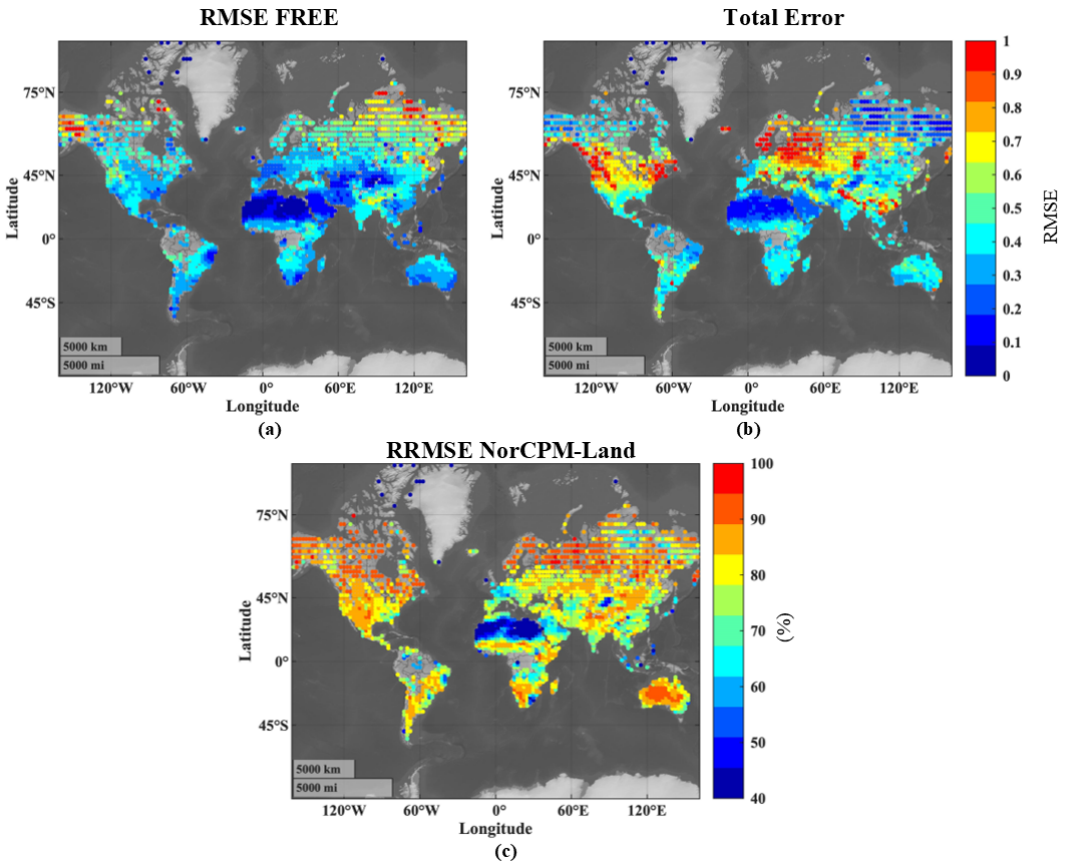

Figure 2. Depicts error indices for (a) FREE in kg/m^2, (b) Total model and observation error as indicated in Eqn. 8 in NorCPM-Land in kg/m^2, (c) Percentage reduction in RMSE in NorCPM-Land.

Figure 3 shows the reliability index for FREE and NorCPM-Land respectively. We can notice that the system is strongly over dispersive (meaning that it overestimates its error) – most particularly at northern hemisphere mid-latitudes (except few regions which are under dispersive such as northeast Asia and Alaska). We can notice that FREE is already overdispersive with a global mean value of about 0.55 meaning that the spread is nearly twice the error of the ensemble mean - the observation error is much smaller than the ensemble spread. In the assimilation system the reliability is degraded, reaching a global average of about 0.19. This implies that the spread is now about 5 times larger than the error of the ensemble mean. While the spread of NorCPM-Land is smaller than in FREE, the RMSE has reduced more. We think that the reason for this is twofold. First, during the daily assimilation cycle, an ensemble of atmospheric fluxes (at every 3 hourly interval) with unsynchronised internal variability provides the atmospheric fluxes. While the ensemble mean is poorly affected by that (error of the fluxes cancels out), the ensemble spread will grow rapidly. Second, the bias correction strategy (i.e. CDF matching) contributes actively to the worsening of the reliability. The CDF matching function is computed a-priori from FREE, which overestimates the spread because of the climatological fluxes. As such, using the function as a reference during the assimilation tends to sustain a too-large spread during analysis while the error of the mean is reduced. Therefore, in our system, assimilation reduces error in the mean more than it reduces the spread causing a degradation in the reliability index.

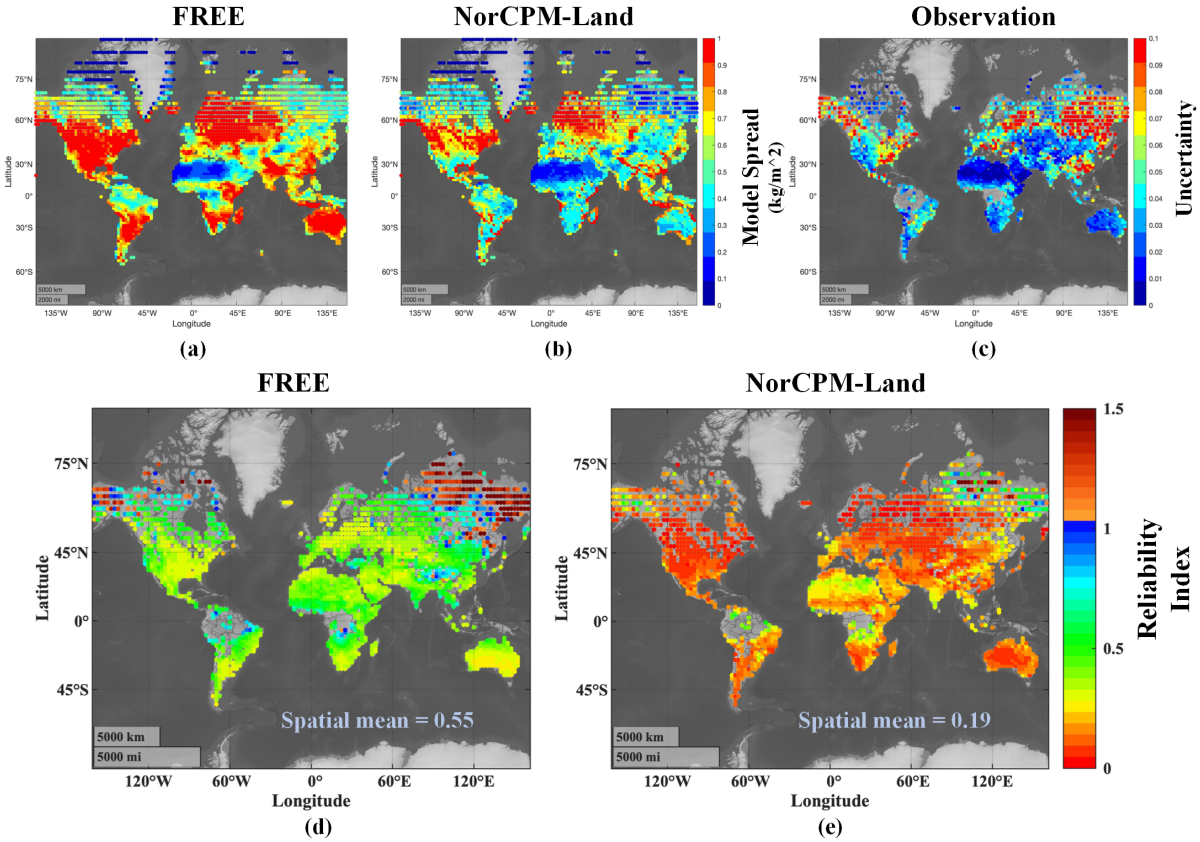

Figure 3. Depicts (a) ensemble spread for FREE (b), ensemble spread for NorCPM-Land (c), observation uncertainty (d) reliability index for FREE (e), and reliability index for NorCPM-Land.

We foresee that in future versions of the system where fluxes will be provided by a version of NorCPM with constrained atmospheric variability, the reliability of the FREE run would be

improved. If the reliability of FREE is good, then CDF matching will not cause a degradation of reliability. If not, one may use adaptive inflation (El Gharamti, 2018), which can inflate or deflate the spread based on reliability statistics. Another approach is to estimate the CDF function from the evolving ensemble -also known as Gaussian anamorphosis (Bertino and Evensen 2003).

5.2 Comparison with independent Soil Moisture Estimates

The simulated daily average SM from NorCPM-Land is validated with independent in-situ observations from ISMN (section 3.3.1). FREE has a large error in SM over west United states of America and over Sahel in Africa (Figure 4a). These regions are of primary interest for improving sub-seasonal forecast, as they have strong coupling with the atmosphere. NorCPM-Land reduce considerably the error - overall by 10.5% globally and by 40 % over parts of USA, the Sahel along with other regions. This accuracy is compared to two well-established land reanalysis products which are ERA5-Land and Global Land Data Assimilation System (GLDAS). We can notice that NorCPM-Land shows lower RMSE than both products, but it should be reminded that those reanalyses products do not assimilate SM explicitly. The domain average of reanalysis products and NorCPM-Land are shown in Figure 4c-e.

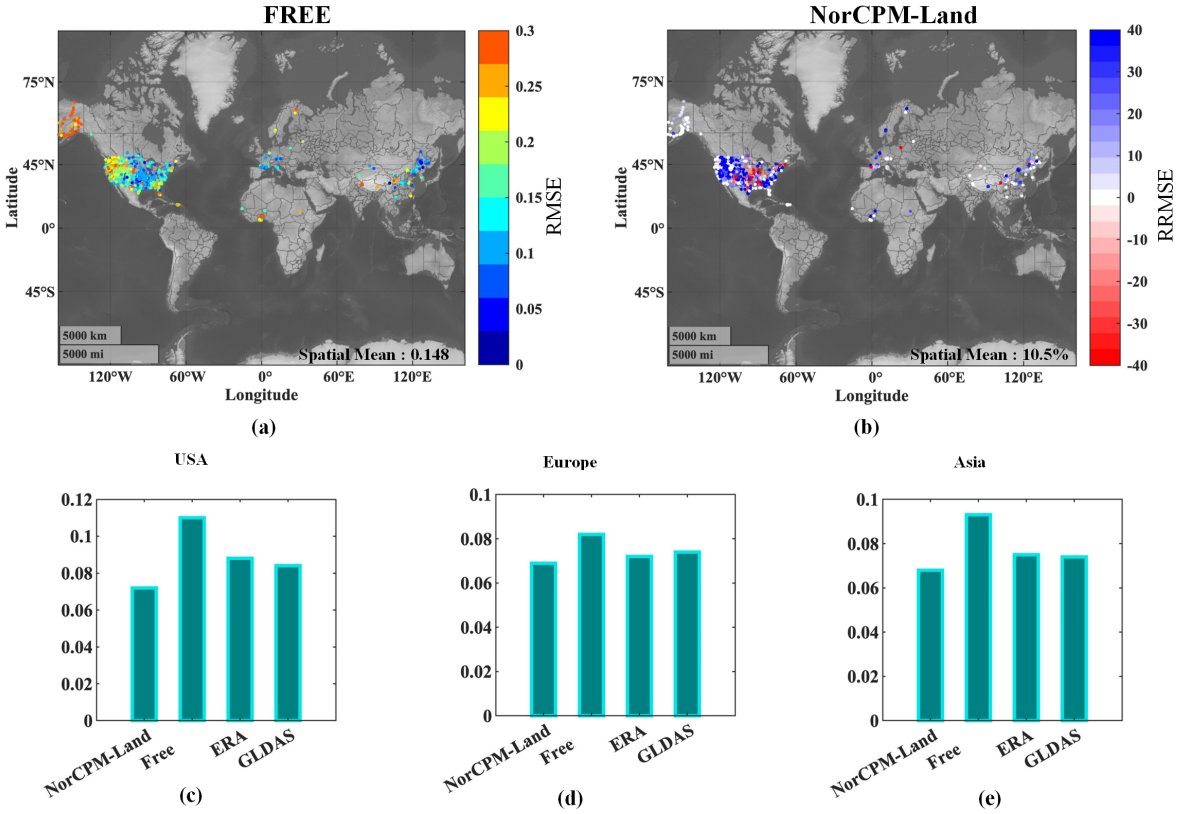

Figure 4. Daily average RMSE for FREE (a), RRMSE of NorCPM-Land (blue color indicates regions with improvement), (c) domain average of RMSE over USA, (d) domain average of RMSE over Europe, (e) domain average of RMSE over Asia

To assess performance of NorCPM-Land compared to FREE in the rest of the domain and where independent data are not available, or for other quantity than soil moisture, we use the ERA5-land. Figure 5a shows the pointwise RMSE of monthly average SM from FREE compared to ERA5-L. This is computed after removing the monthly climatology (seasonal cycle) from the simulated SM, therefore the RMSE computed here is termed as deseasoned RMSE. The assimilation significantly improved SM (see Figure 5b) particularly, over dry regions of the Sahara, Mexico, and Australia. The improvement in RMSE is shown in terms of RRMSE in percentage. NorCPM-Land improves the simulation skill of SM by reducing an error of 12.75% globally when compared to FREE run (Figure 5b).

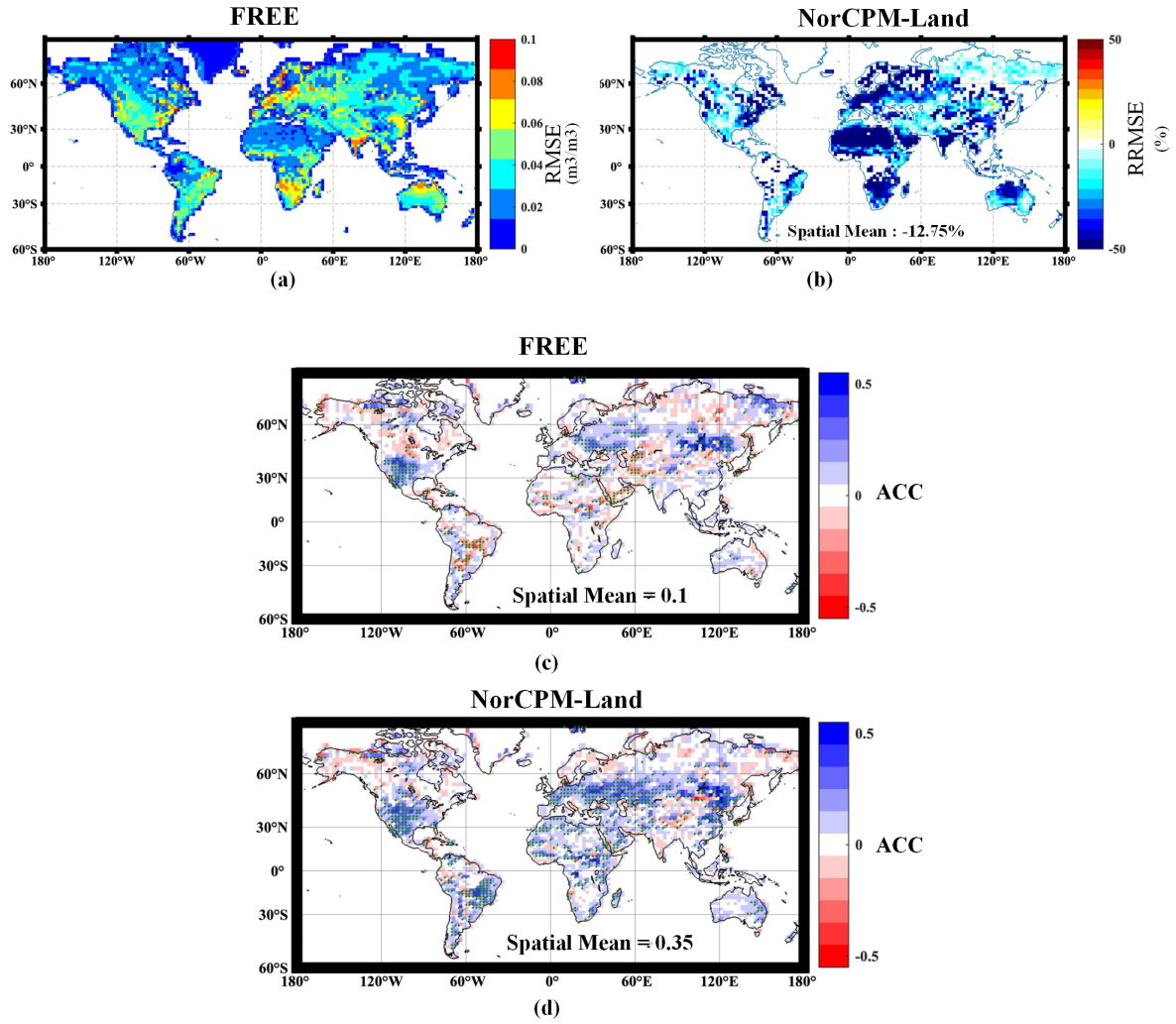

Figure 5. Deseasoned monthly average RMSE of FREE (a), RRMSE of NorCPM-Land (b) where cool colors indicates regions with reduced RMSE and warm color indicates degradation of regions. ACC of monthly averaged SM with respect to ERA for (c) FREE, (d) NorCPM-Land (Grid with significant correlation coefficient is marked with green dot)

We analyse anomaly correlation coefficient (ACC) (see Figure 5c,d), which is computed after removing the mean and so is not directly influenced by model bias. In FREE the 30 members

are only constrained by external forcing. There are some significant changes in places where trends caused by climate change has been most noticeable. The improvement in SM estimates in NorCPM-Land after assimilation is evident from the ACC in Figure 5d as compared to FREE (Figure 5c). This analysis demonstrates that SM assimilation enhances ACC after assimilation, with a global average of 0.35 for NorCPM-Land against 0.1 for FREE run. In particular, the improvement is more noticeable across Sahel, which has demonstrated enhanced ACC and lower RMSE (Figure 5b) in NorCPM-Land.

5.3 Improvement in Land-Atmospheric Coupling

The latent heat flux (LHF) in the land-atmosphere energy exchange is directly related to evaporation, which moistens the atmosphere. Precipitation causes the atmosphere to dry by releasing latent heat into the atmosphere, resulting in a strong heating source and moist convection. One of the important variables influencing the latent heat flux is SM. We first evaluate the estimates of LHF with reference to ERA5-Land data to provide a dynamical assessment on the impact of the assimilation. This analysis will indicate the improvement in LHF following improvement in the SM assimilation framework. Figure 6a indicates RMSE in LHF in FREE after removing monthly climatology (deseasoned RMSE). The impact of improved SM estimates after assimilated propagates into LHF with reduced RMSE, as shown in Figure 6b. The domain average of reduction in LHF is 2.1% after assimilation of SM but is more evident over parts of Sahel and USA which has strong land-atmospheric coupling and where it reaches values up to 30 %. There are also a few regions where the error for LHF has increased following SM assimilation. However, most of these areas exhibit lower RMSE (Figure 5b) and greater ACC (Figure 5d) than FREE run. Therefore, these regions exhibiting deteriorating performance must be studied further to determine the factors triggering this deterioration.

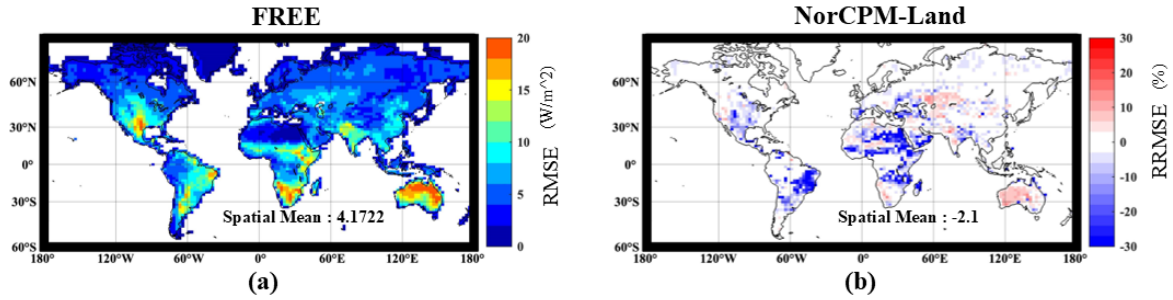

Figure 6. Spatial variability of monthly deseasoned LHF RMSE from FREE (a), and the reduction of RMSE by SM assimilation in NorCPM-Land – blue color indicates regions with improvement- (b).

The improvement in land-atmosphere feedback is further evaluated by computing ACI (See Section 4, Eqn. 9). This analysis is carried out for four seasons: March to May (MAM), June to August (JJA), September to November (SON), and December to February (DJF). During MAM there is long precipitation season over east Africa which has a strong coupling with latent heat flux as seen in reference ACI (Figure 7a). However, FREE (Figure 7c) does not exhibit such coupling. The improved latent heat flux after SM assimilation Improves this coupling (Figure 7c). Some of the major locations showing improvement in coupling after SM assimilation are highlighted by

circles. Similarly, During JJA there is in increase coupling strength over India after SM assimilation (Figure 7e) matching with ERA5-Land coupling map (Figure 7d). Similarly, coupling strength increases over Sahel (highlighted in black rectangle) during JJA. Furthermore, during SON the influence of latent heat flux on precipitation improves with reference over the USA as observed in Figure 7g, h. A consistent improvement is observed over Australia, particularly during DJF (Figure 7k,j).

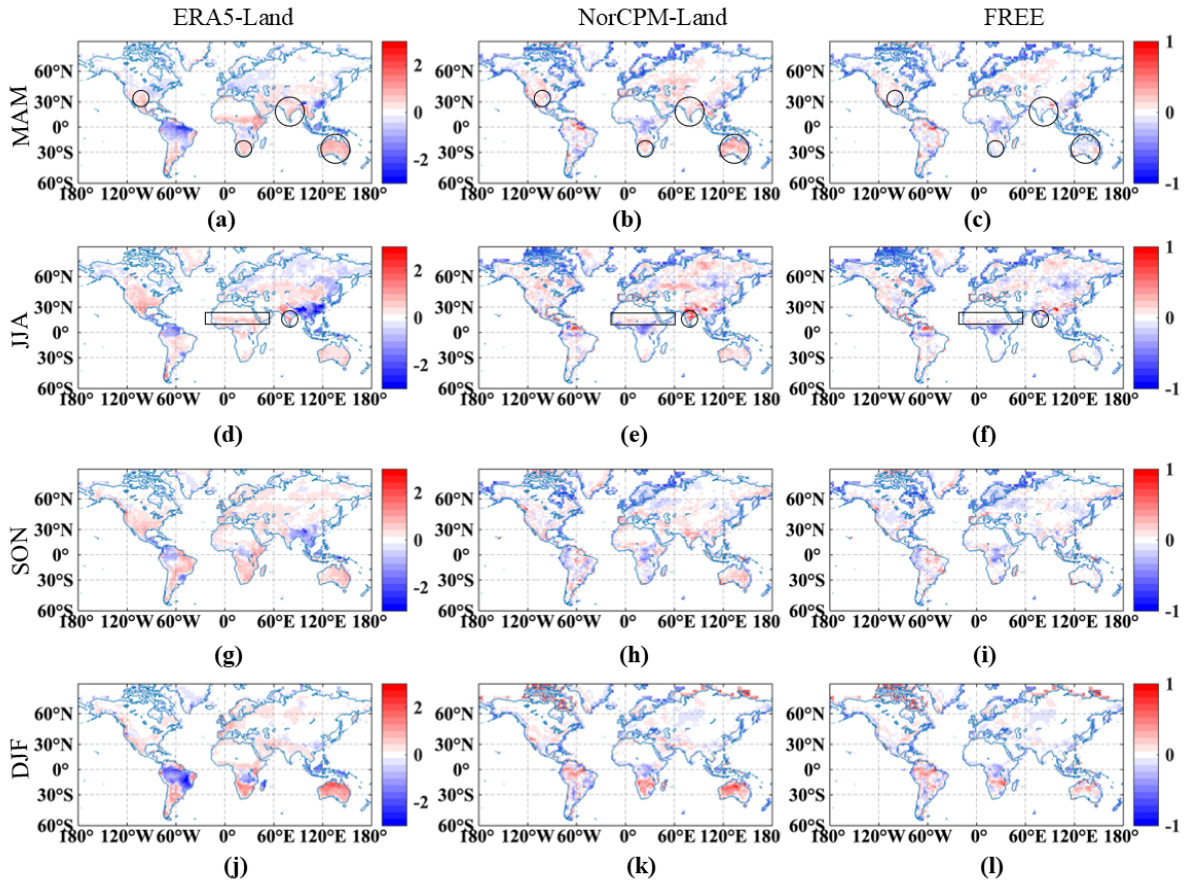

Figure 7. Atmospheric Coupling Index for ERA5-Land (a,d,g,j), (b,e,h,k) NorCPM-Land, and (c,f,i,l) FREE for different seasons. Note different scales for ERA5-Land and the NorCPM and FREE results.

5.4 Runoff

To assess the potential of improving runoff estimates by assimilating SM, nonrouted observational gridded monthly runoff data from GRUN (details in section 3.3.3) are utilized as an independent source of information to compare the results. To compare with GRUN runoff data, total runoff is computed as the sum of surface and subsurface runoff for each grid cell for a duration of 34 years from 1980 to 2014. Figure 8a indicates RMSE in runoff estimates from FREE. The reduction in RMSE after assimilation of SM is indicated in Figure 8b. Though there is an improvement in surface runoff estimates at global mean of 0.31mm/month, there is no large reduction over major basins (such as Amazon, Mississippi, Congo, etc.). This is because another

key component influencing runoff is precipitation, which is not constrained or improved in the historical runs of NorESM in this study.

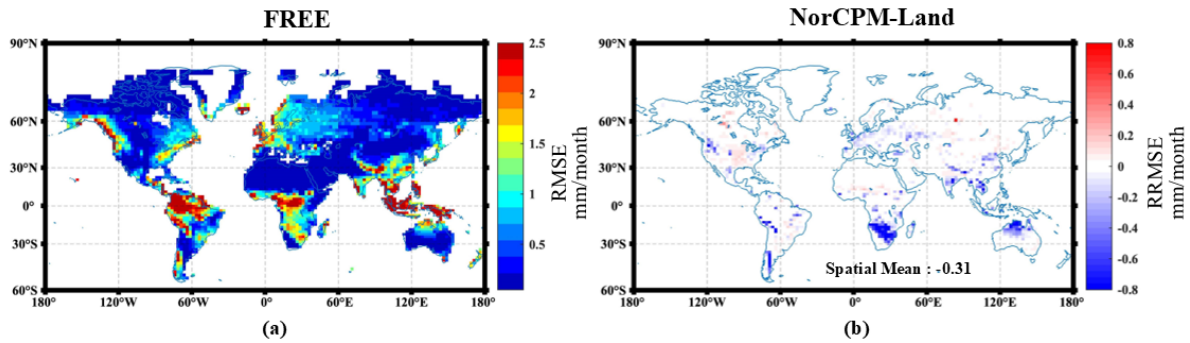

Figure 8. Depicts RMSE in surface runoff with reference to GRUN for (a) FREE, (b) NorCPM-Land (blue color indicates regions with improvement)

5.5 Net Primary Productivity

With reference to independent measurement from satellite data (details provided in section 3.3.4), we assess the propagation of enhanced SM states in NorCPM-Land on simulating NPP. It is well known that the availability of SM can effect plant productivity and is most frequently employed to assess vegetation dryness stress (Liu et al., 2020). If plants are unable to sustain turgor, decreased SM may result in biophysical drought stress, which would lower primary production by closing stomata. Alternately, lower SM may limit nutrient mass movement in the soil and microbial activity, reducing nitrogen mineralization and availability and thereby reducing primary output. Figure 9a depicts the RMSE in FREE. Substantial error is detected in the tropical rainforest of the Congo basin, as well as in other places. Improved SM condition in NorCPM-Land minimizes inaccuracy in NPP over a few locations. Figure 9b shows that the RMSE of NPP is reduced by SM assimilation. However, it has less of an influence on huge thick forests (such as those in the Congo basin) since SM is not assimilated in densely vegetated areas as mentioned in section 2.5. After SM assimilation, an overall reduction in global average NPP error of 0.28 $gC/m^2/day$ (around 9.3% reduction) is observed.

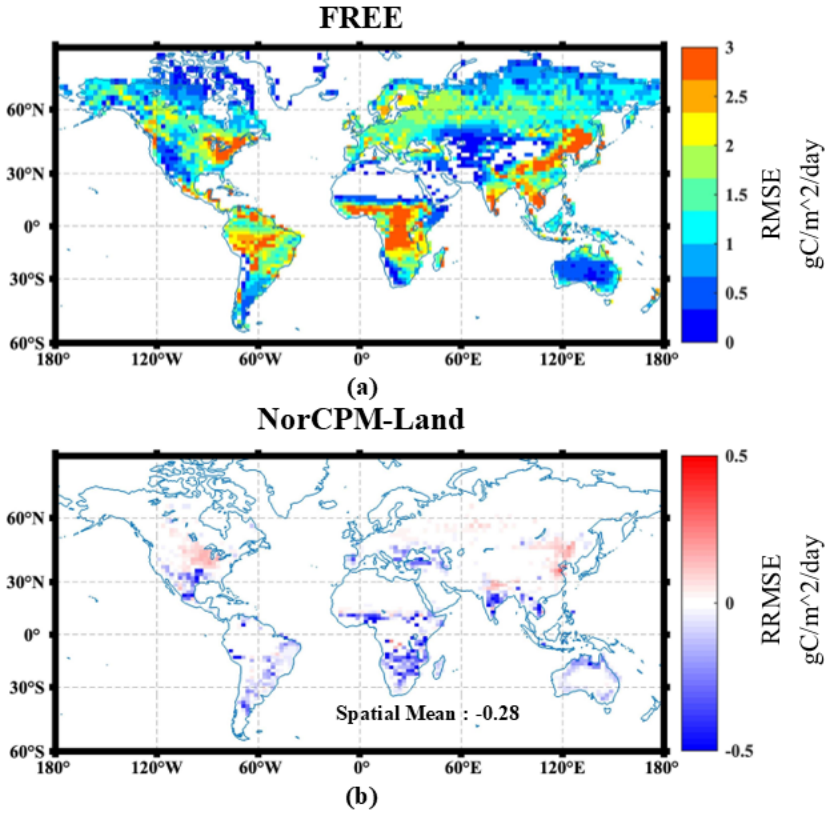

Figure 9. RMSE of monthly NPP compared to MODIS NPP for (a) FREE, (b) and reduction of RMSE from FREE in NorCPM-Land (blue color indicates regions with improvement)

6 Summary and Conclusions

In this study, we developed a new global land reanalysis system (NorCPM-Land) that simulates surface soil moisture and other land surface water and energy flux components by assimilating daily the blended satellite SM data from ESA CCI. The merging of multi-satellite data in the ESA CCI has enabled this study to perform daily assimilation. Assimilating SM considerably improved the skill of CLM in simulating land surface states. The system is run offline but uses fluxes from an ensemble of the same coupled system as used for running the NorCPM climate predictions and uses CDF matching to handle the mismatch between the model SM and ESA-CCI observations. As such the reanalysis can provide improved land initialization and maintains the numerical compatibility of NorCPM-Land with NorCPM and avoids numerical shocks during initialization of predictions with the same model.

Using NorCPM-Land, an improved land initial state is produced over a period of four decades, from 1980 to 2019 inclusive. The system depends on stochastic assimilation of SM data using the EnSRF into CLM. The system is overdispersive for SM, and the overdispersion already present in the ensemble without assimilation is degraded. We have identified different factors that contribute to this large ensemble spread, including (i) bias correction approach of matching the CDF of CCI SM with FREE run prior to assimilation, (ii) adopting a constant inflation factor, and

(iii) unconstrained atmospheric forcing for offline CLM run. The CDF matching approach converts observations to model (FREE) climatology. After assimilation step, the analysis states are attracted to the substantial variability of the FREE ensemble spread. As a result, despite the reduction in error of the ensemble mean after assimilation, it has a higher spread than error causing over dispersive reliability index in most of the regions. The conventional CDF matching approach assumes that the model and observation biases are stationary, making it difficult to adapt to dynamic changes in the bias characteristics. To overcome this in future work we intend to adapt flow dependent bias correction techniques. We further anticipate that using adaptive inflation and adding an atmospheric constraint on the system that provide the ensemble of atmospheric flux would improve reliability in the future versions of the system.

In comparison to independent datasets, NorCPM-Land enhances the ability to capture the spatiotemporal dynamics of SM. Validation of results using in-situ SM data shows a 10.5% reduction in error for NorCPM-Land simulated SM compared to FREE. NorCPM-Land SM estimations consistently outperform GLDAS and ERA5-Land on a global scale. In addition, the NorCPM-Land decreases the error by 12.75 on a global scale with reference to ERA5-Land when compared to FREE SM estimations. This study also highlights the added value of improving SM estimates in other land surface state variables. The NorCPM-Land minimizes the error in latent heat flux, an important variable in the energy exchange between land and atmosphere. The enhancements in latent heat flux are most evident in midlatitudes, namely over the United States of America, Sahel, and India, which have considerable land-atmosphere coupling. When evaluating the land-atmosphere coupling of NorCPM-Land, ERA5-Land is used as a reference. The results of NorCPM-Land consistently reflect the spatial coupling pattern of ERA for all four seasons. In some regions, the improvement in SM condition substantially improves runoff estimates when compared to GRUN runoff reconstruction data, but the uncertainty in precipitation forcing limits the extent of the improvement. The improvement is also observed in interaction between SM and vegetation productivity with respect to NPP. When compared with satellite NPP as reference, NorCPM-Land indicated a reduction in error of 9.3% in comparison to FREE. This indicates the contribution of SM assimilation in improving the terrestrial carbon cycle and vegetation dynamics.

In conclusion, the current re-analysis system has been thoroughly validated and we will test its potential to provide land initial condition to NorCPM to enhance the skill of S2S predictions. In addition, future work will focus on integrating different data for other land surface variables, such as snow and skin temperature, as well as improved forcing data. This will aid in the improvement of high-latitude prediction skills.

Acknowledgements

The research was partly funded by Research Council under the NORKLIMA research programme (EPOCASA; 229774/E10), the Climate Futures research centre (grant 309562). This work has also received a grant for computer time from the Norwegian Program for supercomputing (NOTUR2, project no. NN9039K) and a storage grant (NORSTORE, NS9039K).

Open Research

Data Availability Statement

The code of Norwegian Earth System Model (NorESM), Norwegian Climate Prediction Model (NorCPM version1) are available online on the Norwegian Earth System Modeling hub (https://github.com/NorESMhub). Specific details about NorCPM can be found in the website (https://wiki.app.uib.no/norcpm/index.php/Norwegian_Climate_Prediction_Model). The ESA CCI merged soil moisture data can be obtained from the climate change initiative website (https://www.esa-soilmoisture-cci.org). The reference data from ERA-Land can be obtained from the Copernicus web services (https://cds.climate.copernicus.eu/cdsapp#!/dataset/reanalysis-era5-land?tab=form). The insitu soil moisture from International Soil Moisture network can be found at data hosting facility (https://ismn.earth/en/). The Global runoff dataset can be found online at https://doi.org/10.6084/m9.figshare.9228176. The GLDAS data can be obtained from (https://disc.gsfc.nasa.gov/datasets?keywords=GLDAS). The Net Primary Productivity dataset can be found online at https://lpdaac.usgs.gov/data_access/.

References

Alyaari, A., Dayau, S., Chipeaux, C., Aluome, C., Kruszewski, A., Loustau, D., & Wigneron, J.P. (2018). The AQUI Soil Moisture Network for Satellite Microwave Remote Sensing Validation in South-Western France. *Remote. Sens., 10*, 1839.

Assmann, K.M., Bentsen, M., Segschneider, J., & Heinze, C. (2009). An isopycnic ocean carbon cycle model. *Geoscientific Model Development, 3*, 143-167.

Bentsen, M., Bethke, I., Debernard, J.B., Iversen, T., Kirkevåg, A., Seland, Ø., Drange, H., Roelandt, C., Seierstad, I.A., Hoose, C., & Kristjánsson, J.E. (2013). The Norwegian Earth System Model, NorESM1-M – Part 1: Description and basic evaluation of the physical climate. *Geoscientific Model Development, 6*, 687-720.

Bertino, L., Evensen, G., & Wackernagel, H. (2003). Sequential Data Assimilation Techniques in Oceanography. *International Statistical Review / Revue Internationale de Statistique*, *71*(2), 223–241. http://www.jstor.org/stable/1403885

Bethke, I., Wang, Y., Counillon, F., Keenlyside, N.S., Kimmritz, M., Fransner, F., Samuelsen, A., Langehaug, H.R., Svendsen, L., Chiu, P., Passos, L., Bentsen, M., Guo, C., Gupta, A.K., Tjiputra, J.F., Kirkevåg, A., Oliviè, D.J., Seland, Ø., Solsvik Vågane, J., Fan, Y., & Eldevik, T. (2021). NorCPM1 and its contribution to CMIP6 DCPP. Geoscientific Model Development.

Bleck, R., Rooth, C.G., Hu, D., & Smith, L.T. (1992). Salinity-driven Thermocline Transients in a Wind- and Thermohaline-forced Isopycnic Coordinate Model of the North Atlantic. *Journal of Physical Oceanography, 22*, 1486-1505.

Carver, K.R., Elachi, C., & Ulaby, F.T. (1985). Microwave remote sensing from space. *Proceedings of the IEEE, 73*, 970-996.

683 Chen, F., Mitchell, K.E., Schaake, J.C., Xue, Y., Pan, H.L., Koren, V., Duan, Q., Ek, M.B., &
684 Betts, A.K. (1996). Modeling of land surface evaporation by four schemes and
685 comparison with FIFE observations. *Journal of Geophysical Research, 101*, 7251-7268.

686 Cosby, B., Hornberger, G.M., Clapp, R.B., & Ginn, T.R. (1984). A Statistical Exploration of the
687 Relationships of Soil Moisture Characteristics to the Physical Properties of Soils. *Water*
688 *Resources Research, 20*, 682-690.

689 Counillon, F., Bethke, I., Keenlyside, N.S., Bentsen, M., Bertino, L., & Zheng, F. (2014).
690 Seasonal-to-decadal predictions with the ensemble Kalman filter and the Norwegian
691 Earth System Model: a twin experiment. Tellus A: Dynamic Meteorology and
692 Oceanography, 66.

693 Counillon, F., Keenlyside, N.S., Bethke, I., Wang, Y., Billeau, S., Shen, M., & Bentsen, M.
694 (2016). Flow-dependent assimilation of sea surface temperature in isopycnal coordinates
695 with the Norwegian Climate Prediction Model. *Tellus A: Dynamic Meteorology and*
696 *Oceanography, 68*. DOI: 10.3402/tellusa.v68.32437

697 Courtier, P., Thepaut, J., & Hollingsworth, A. (1994). A strategy for operational implementation
698 of 4D-Var, using an incremental approach. *Quarterly Journal of the Royal*
699 *Meteorological Society, 120*, 1367-1387.

700 Dai, Y., Zeng, X., Dickinson, R.E., Baker, I.T., Bonan, G.B., Bosilovich, M.G., Denning, A.S.,
701 Dirmeyer, P.A., Houser, P.R., Niu, G., Oleson, K.W., Schlosser, C., & Yang, Z. (2003).
702 The Common Land Model. *Bulletin of the American Meteorological Society, 84*, 1013-
703 1023.

704 de Rosnay, P., Drusch, M., Vasiljevic, D., Balsamo, G., Albergel, C., & Isaksen, L. (2013). A
705 simplified Extended Kalman Filter for the global operational soil moisture analysis at
706 ECMWF. Quarterly Journal of the Royal Meteorological Society, 139.

707 Dente, L., Su, Z., & Wen, J. (2012). Validation of SMOS Soil Moisture Products over the Maqu
708 and Twente Regions. *Sensors (Basel, Switzerland), 12*, 9965 - 9986.

709 Dirmeyer, P.A., & Halder, S. (2016). Sensitivity of Numerical Weather Forecasts to Initial Soil
710 Moisture Variations in CFSv2. Weather and Forecasting, 31, 1973-1983.

711 Dirmeyer, P.A., Halder, S., & Bombardi, R.J. (2018). On the Harvest of Predictability From
712 Land States in a Global Forecast Model. Journal of Geophysical Research: Atmospheres,
713 123, 13,111 - 13,127.

714 Dorigo, W.A., Oevelen, P.J., Wagner, W., Drusch, M., Mecklenburg, S., Robock, A., & Jackson,
715 T.J. (2011). A New International Network for in Situ Soil Moisture Data. *Eos,*
716 *Transactions American Geophysical Union, 92*, 141-142.

717 Drusch, M., Scipal, K., de Rosnay, P., Balsamo, G., Andersson, E., Bougeault, P., & Viterbo, P.
718 (2009). Towards a Kalman Filter based soil moisture analysis system for the operational
719 ECMWF Integrated Forecast System. *Geophysical Research Letters, 36*.

720 Ducharne, A.; Koster, R.D.; Suarez, M.J.; Stieglitz, M.; Kumar, P. A catchment-based approach
721 to modeling land surface processes in a GCM, Part 2, Parameter estimation and model
722 demonstration. *J. Geophys. Res. Atmos.***2000**, *105*, 24823–24838.

El Gharamti, M. (2018). Enhanced Adaptive Inflation Algorithm for Ensemble Filter, Monthly Weather Review, 146(2), 623-640

Entekhabi, D., Njoku, E.G., O'neill, P.E., Kellogg, K.H., Crow, W.T., Edelstein, W.N., Entin, J.K., Goodman, S.D., Jackson, T.J., Johnson, J.T., Kimball, J.S., Piepmeier, J.R., Koster, R.D., Martin, N., McDonald, K., Moghaddam, M., Moran, M.S., Reichle, R.H., Shi, J., Spencer, M.W., Thurman, S.W., Tsang, L., & Zyl, J.J. (2010). The Soil Moisture Active Passive (SMAP) Mission. *Proceedings of the IEEE, 98*, 704-716.

Evensen, G. (2003). The Ensemble Kalman Filter: theoretical formulation and practical implementation. *Ocean Dynamics, 53*, 343-367.

Fischer, E.M., Seneviratne, S.I., Vidale, P.L., Lüthi, D., & Schär, C.M. (2007). Soil Moisture–Atmosphere Interactions during the 2003 European Summer Heat Wave. *Journal of Climate*, 20, 5081-5099.

Fortin, V., Abaza, M., Anctil, F., & Turcotte, R. (2014). Why Should Ensemble Spread Match the RMSE of the Ensemble Mean? *Journal of Hydrometeorology*, *15*(4), 1708-1713.

Gaiser, P.W., Germain, K.M., Twarog, E.M., Poe, G.A., Purdy, W.E., Richardson, D., Grossman, W., Jones, W.L., Spencer, D.A., Golba, G., Cleveland, J., Choy, L.W., Bevilacqua, R.M., & Chang, P.S. (2004). The WindSat spaceborne polarimetric microwave radiometer: sensor description and early orbit performance. *IEEE Transactions on Geoscience and Remote Sensing, 42*, 2347-2361.

Gent, P. R., Danabasoglu, G., Donner, L. J., Holland, M. M., Hunke, E. C., Jayne, S. R., Lawrence, D. M., Neale, R. B., Rasch, P. J., Vertenstein, M., Worley, P. H., Yang, Z., & Zhang, M. (2011). The Community Climate System Model Version 4, *Journal of Climate*, *24*(19), 4973-4991.

Ghiggi, G., Humphrey, V., Seneviratne, S.I., & Gudmundsson, L. (2019). GRUN: an observation-based global gridded runoff dataset from 1902 to 2014. *Earth System Science Data*.

González-Zamora, Á., Sánchez, N., Pablos, M., & Martínez-Fernández, J. (2019). CCI soil moisture assessment with SMOS soil moisture and in situ data under different environmental conditions and spatial scales in Spain. *Remote Sensing of Environment*.

Guo, Z., Dirmeyer, P. A., and DelSole, T. (2011), Land surface impacts on subseasonal and seasonal predictability, *Geophys. Res. Lett.*, 38, L24812, doi:10.1029/2011GL049945.

Hallikainen, M., Ulaby, F.T., Dobson, M.C., El-rayes, M., & Wu, L. (1985). Microwave Dielectric Behavior of Wet Soil-Part 1: Empirical Models and Experimental Observations. *IEEE Transactions on Geoscience and Remote Sensing, GE-23*, 25-34.

Hersbach, H., Bell, B., Berrisford, P., Hirahara, S., Horányi, A., Muñoz-Sabater, J., Nicolas, J., Peubey, C., Radu, R., Schepers, D., Simmons, A., Soci, C., Abdalla, S., Abellan, X., Balsamo, G., Bechtold, P., Biavati, G., Bidlot, J., Bonavita, M., Chiara, G.D., Dahlgren, P., Dee, D., Diamantakis, M., Dragani, R., Flemming, J., Forbes, R.G., Fuentes, M., Geer, A.J., Haimberger, L., Healy, S.B., Hogan, R.J., Holm, E.V., Janisková, M., Keeley, S.P., Laloyaux, P., Lopez, P., Lupu, C., Radnoti, G., Rosnay, P.D., Rozum, I., Vamborg, F., Villaume, S., & Thepaut, J. (2020). The ERA5 global reanalysis. *Quarterly Journal of the Royal Meteorological Society, 146*, 1999 - 2049.

765 Holland, M.M., Bailey, D.A., Briegleb, B.P., Light, B., & Hunke, E.C. (2012). Improved sea ice
766 shortwave radiation physics in CCSM4: The impact of melt ponds and aerosols on Arctic
767 Sea ice. *Journal of Climate, 25*, 1413-1430.

768 Hurrell, J.W., Holland, M.M., Gent, P.R., Ghan, S.J., Kay, J.E., Kushner, P.J., Lamarque, J.,
769 Large, W., Lawrence, D.M., Lindsay, K., Lipscomb, W.H., Long, M.C., Mahowald,
770 N.M., Marsh, D.R., Neale, R.B., Rasch, P.J., Vavrus, S.J., Vertenstein, M., Bader, D.C.,
771 Collins, W.D., Hack, J.J., Kiehl, J.T., & Marshall, S.J. (2013). The Community Earth
772 System Model: A Framework for Collaborative Research. *Bulletin of the American*
773 *Meteorological Society, 94*, 1339-1360.

774 Ikonen, J., Smolander, T., Rautiainen, K., Cohen, J., Lemmetyinen, J., Salminen, M., &
775 Pulliainen, J. (2018). Spatially Distributed Evaluation of ESA CCI Soil Moisture
776 Products in a Northern Boreal Forest Environment.

777 Imaoka, K., M. Kachi, M. Kasahara, K. Nakagawa, and T. Oki (2010), Instrument performance
778 and calibration of AMSR-E and AMSR2, paper presented at International Archives of the
779 Photogrammetry, Remote Sensing and Spatial Information Science, ISPRS, Kyoto,
780 Japan.

781 Iversen, T., Bentsen, M., Bethke, I., Debernard, J.B., Kirkevåg, A., Seland, Ø., Drange, H.,
782 Kristjánsson, J.E., Medhaug, I., Sand, M., & Seierstad, I.A. (2012). The Norwegian Earth
783 System Model, NorESM1-M – Part 2: Climate response and scenario
784 projections. *Geoscientific Model Development, 6*, 389-415.

785 Jensen, K.H., & Refsgaard, J.C. (2018). HOBE: The Danish Hydrological Observatory. *Vadose*
786 *Zone Journal, 17*.

787 Karspeck, AR, Danabasoglu G, Anderson J, et al. A global coupled ensemble data assimilation
788 system using the Community Earth System Model and the Data Assimilation Research
789 Testbed. Q J R Meteorol Soc. 2018; 144: 2404– 2430. https://doi.org/10.1002/qj.3308

790 Kerr, Y.H., Waldteufel, P., Wigneron, J.P., Delwart, S., Cabot, F., Boutin, J., Escorihuela, M.J.,
791 Font, J., Reul, N., Gruhier, C., Juglea, S.E., Drinkwater, M.R., Hahne, A., Martín-Neira,
792 M., & Mecklenburg, S. (2010). The SMOS Mission: New Tool for Monitoring Key
793 Elements ofthe Global Water Cycle. *Proceedings of the IEEE, 98*, 666-687.

794 Kirkevåg, A., Iversen, T., Seland, Ø., Hoose, C., Kristjánsson, J.E., Struthers, H., Ekman, A.M.,
795 Ghan, S.J., Griesfeller, J., Nilsson, E.D., & Schulz, M. (2013). Aerosol–climate
796 interactions in the Norwegian Earth System Model – NorESM1-M. *Geoscientific Model*
797 *Development, 6*, 207-244.

798 Koster, R.D., & Suárez, M.J. (1992). Modeling the land surface boundary in climate models as a
799 composite of independent vegetation stands. *Journal of Geophysical Research, 97*, 2697-
800 2715.

801 Koster, R.D., Dirmeyer, P.A., Guo, Z., Bonan, G.B., Chan, E., Cox, P.M., Gordon, C.T., Kanae,
802 S., Kowalczyk, E.A., Lawrence, D.M., Liu, P., Lu, C., Malyshev, S., Mcavaney, B.J.,
803 Mitchell, K., Mocko, D.M., Oki, T., Oleson, K.W., Pitman, A.J., Sud, Y.C., Taylor,
804 C.M., Verseghy, D.L., Vasic, R., Xue, Y., & Yamada, T.J. (2004). Regions of Strong
805 Coupling Between Soil Moisture and Precipitation. *Science, 305*, 1138 - 1140.

Koster, R.D., Mahanama, S., Yamada, T.J., Balsamo, G., Berg, A.A., Boisserie, M.A., Dirmeyer, P.A., Doblas-Reyes, F., Drewitt, G., Gordon, C.T., Guo, Z., Jeong, J., Lawrence, D.M., Lee, W., Li, Z.L., Luo, L., Malyshev, S., Merryfield, W.J., Seneviratne, S.I., Stanelle, T., van den Hurk, B., Vitart, F., & Wood, E.F. (2010). Contribution of land surface initialization to subseasonal forecast skill: First results from a multi-model experiment. *Geophysical Research Letters, 37*.

Koster, R.D.; Suarez, M.J.; Ducharne, A.; Stieglitz, M.; Kumar, P. A catchment-based approach to modeling land surface processes in a GCM, Part 1, Model Structure. *J. Geophys. Res. Atmos.* **2000**, *105*, 24809–24822.

Kumar, S. V., Reichle, R. H., Harrison, K. W., Peters-Lidard, C. D., Yatheendradas, S., and Santanello, J. A. (2012), A comparison of methods for a priori bias correction in soil moisture data assimilation, *Water Resour. Res.*, 48, W03515, doi:10.1029/2010WR010261.

Kumar, S.V., Reichle, R.H., Harrison, K.W., Peters-Lidard, C.D., Yatheendradas, S., & Santanello, J.A. (2011). A comparison of methods for a priori bias correction in soil moisture data assimilation. *Water Resources Research, 48*.

Lawrence, D. M., & Slater, A. G. (2008). Incorporating organic soil into a global climate model. *Climate Dynamics*, *30*, 145-160. doi:10.1007/s00382-007-0278-1

Liang, X., Lettenmaier, D.P., Wood, E.F., & Burges, S.J. (1994). A simple hydrologically based model of land surface water and energy fluxes for general circulation models. *Journal of Geophysical Research, 99*, 14415-14428.

Liu, L., Gudmundsson, L., Hauser, M. *et al.* Soil moisture dominates dryness stress on ecosystem production globally. *Nat Commun* **11**, 4892 (2020). https://doi.org/10.1038/s41467-020-18631-1

Mariotti, A., Ruti, P.M., & Rixen, M. (2018). Progress in subseasonal to seasonal prediction through a joint weather and climate community effort. *npj Climate and Atmospheric Science, 1*, 1-4.

McColl, K.A., Alemohammad, S.H., Akbar, R., Konings, A.G., Yueh, S.H., & Entekhabi, D. (2017). The global distribution and dynamics of surface soil moisture. *Nature Geoscience, 10*, 100-104.

Meehl, G.A., Richter, J.H., Teng, H., Capotondi, A., Cobb, K.M., Doblas-Reyes, F.J., Donat, M.G., England, M.H., Fyfe, J.C., Han, W., Kim, H., Kirtman, B., Kushnir, Y., Lovenduski, N.S., Mann, M.E., Merryfield, W.J., Nieves, V., Pegion, K., Rosenbloom, N.A., Sanchez, S.C., Scaife, A.A., Smith, D.M., Subramanian, A.C., Sun, L., Thompson, D.M., Ummenhofer, C.C., & Xie, S. (2021). Initialized Earth System prediction from subseasonal to decadal timescales. *Nature Reviews Earth & Environment, 2*, 340 - 357.

Merryfield, W.J., Baehr, J., Batté, L., Becker, E.J., Butler, A.H., Coelho, C.A., Danabasoglu, G., Dirmeyer, P.A., Doblas-Reyes, F.J., Domeisen, D.I., Ferranti, L., Ilynia, T., Kumar, A., Müller, W.A., Rixen, M., Robertson, A.W., Smith, D.M., Takaya, Y., Tuma, M.P., Vitart, F., White, C.J., Álvarez, M.S., Ardilouze, C., Attard, H.E., Baggett, C.F., Balmaseda, M.A., Beraki, A.F., Bhattacharjee, P.S., Bilbao, R.A., Andrade, F.M., DeFlorio, M.J., Díaz, L.B., Ehsan, M.A., Fragkoulidis, G., Grainger, S., Green, B.W., Hell, M.C., Infanti,

J.M., Isensee, K., Kataoka, T., Kirtman, B., Klingaman, N.P., Lee, J., Mayer, K.J., McKay, R., Mecking, J.V., Miller, D.E., Neddermann, N., Ng, C.H., Ossó, A., Pankatz, K., Peatman, S.C., Pegion, K., Perlwitz, J., Recalde-Coronel, G.C., Reintges, A., Renkl, C., Solaraju-Murali, B., Spring, A., Stan, C., Sun, Y.Q., Tozer, C.R., Vigaud, N., Woolnough, S.J., & Yeager, S.G. (2020). Current and Emerging Developments in Subseasonal to Decadal Prediction. *Bulletin of the American Meteorological Society*.101(6), E869-E896

Müller, O. V., Vidale, P. L., Vannière, B., Schiemann, R., Senan, R., Haarsma, R. J., & Jungclaus, J. H. (2021). Land–Atmosphere Coupling Sensitivity to GCMs Resolution: A Multimodel Assessment of Local and Remote Processes in the Sahel Hot Spot, *Journal of Climate*, *34*(3), 967-985.

Muñoz-Sabater, J., Dutra, E., Agustí-Panareda, A., Albergel, C., Arduini, G., Balsamo, G., Boussetta, S., Choulga, M., Harrigan, S., Hersbach, H., Martens, B., Miralles, D.G., Piles, M., Rodríguez-Fernández, N.J., Zsoter, E., Buontempo, C., & Thepaut, J. (2021). Supplementary material to "ERA5-Land: A state-of-the-art global reanalysis dataset for land applications". *Earth System Science Data*.

Nair, A.S., & Indu, J. (2016). Enhancing Noah Land Surface Model Prediction Skill over Indian Subcontinent by Assimilating SMOPS Blended Soil Moisture. *Remote. Sens., 8*, 976.

Nair, A.S., & Indu, J. (2019). Improvement of land surface model simulations over India via data assimilation of satellite-based soil moisture products. *Journal of Hydrology*, 573, 406-421.

Nair, A.S., Mangla, R., Thiruvengadam, P., & Indu, J. (2020). Remote sensing data assimilation. *Hydrological Sciences Journal-journal Des Sciences Hydrologiques*, 1-33.

Njoku, E.G., Jackson, T.J., Lakshmi, V., Chan, S.T., & Nghiem, S.V. (2003). Soil moisture retrieval from AMSR-E. *IEEE Trans. Geosci. Remote. Sens., 41*, 215-229.

Oleson, K.W., D.M. Lawrence, G.B. Bonan, B. Drewniak, M. Huang, C.D. Koven, S. Levis, F. Li, W.J. Riley, Z.M. Subin, S.C. Swenson, P.E. Thornton, A. Bozbiyik, R. Fisher, E. Kluzek, J.-F. Lamarque, P.J. Lawrence, L.R. Leung, W. Lipscomb, S. Muszala, D.M. Ricciuto, W. Sacks, Y. Sun, J. Tang, Z.-L. Yang, (2013). Technical Description of version 4.5 of the Community Land Model (CLM). Ncar Technical Note NCAR/TN-503+STR, National Center for Atmospheric Research, Boulder, CO, 422 pp, DOI: 10.5065/D6RR1W7M.

Orth, R., & Seneviratne, S.I. (2012). Analysis of soil moisture memory from observations in Europe. Journal of Geophysical Research, 117.

Penny, S.G., & Hamill, T.M. (2017). Coupled Data Assimilation for Integrated Earth System Analysis and Prediction. *Bulletin of the American Meteorological Society, 98*. ES169-ES172.

Reichle, R.H., & Koster, R.D. (2004). Bias reduction in short records of satellite soil moisture. Geophysical Research Letters, 31.

Reichle, Rolf & Koster, Randal. (2004). Bias Reduction in Short Records of Satellite Soil Moisture. Geophysical Research Letters. 31. 10.1029/2004GL020938.

889 Rodell, M., Houser, P.R., Jambor, U., Gottschalck, J., Mitchell, K.E., Meng, C., Arsenault, K.R.,
890 Cosgrove, B., Radakovich, J.D., Bosilovich, M.G., Entin, J.K., Walker, J.P., Lohmann,
891 D., & Toll, D. (2004). The Global Land Data Assimilation System. *Bulletin of the*
892 *American Meteorological Society, 85*, 381-394.

893 Rodwell, M., Lang, S.T., Ingleby, N.B., Bormann, N., Holm, E.V., Rabier, F., Richardson, D.S.,
894 & Yamaguchi, M. (2016). Reliability in ensemble data assimilation. *Quarterly Journal of*
895 *the Royal Meteorological Society, 142*.

896 Santanello, J.A., Dirmeyer, P.A., Ferguson, C.R., Findell, K.L., Tawfik, A.B., Berg, A.M., Ek,
897 M.B., Gentine, P., Guillod, B.P., Heerwaarden, C.C., Roundy, J.K., & Wulfmeyer, V.
898 (2018). Land–Atmosphere Interactions: The LoCo Perspective. *Bulletin of the American*
899 *Meteorological Society*.

900 Santanello, J.A., Jr.; Peters-Lidard, C.D.; Kumar, S.V. Diagnosing the sensitivity of local land-
901 atmosphere coupling via the soil moisture-boundary layer interaction. J. Hydrometeorol.
902 2011, 12, 766–786.

903 Schaefer, G.L., Cosh, M.H., & Jackson, T.J. (2007). The USDA Natural Resources Conservation
904 Service Soil Climate Analysis Network (SCAN). *Journal of Atmospheric and Oceanic*
905 *Technology, 24*, 2073-2077.

906 Seneviratne, S.I.; Corti, T.; Davin, E.L.; Hirschi, M.; Jaeger, E.B.; Lehner, I.; Orlowsky, B.;
907 Teuling, A.J. Investigating soil moisture-climate interactions in a changing climate: A
908 review. Earth Sci. Rev. 2010, 99, 125–161.

909 Seo, E., Lee, M., Jeong, J., Koster, R.D., Schubert, S., Kim, H., Kim, D.H., Kang, H., Kim, H.,
910 MacLachlan, C., & Scaife, A.A. (2018). Impact of soil moisture initialization on boreal
911 summer subseasonal forecasts: mid-latitude surface air temperature and heat wave
912 events. *Climate Dynamics, 52*, 1695-1709.

913 Seo, E., Lee, M., Schubert, S., Koster, R.D., & Kang, H. (2020). Investigation of the 2016
914 Eurasia heat wave as an event of the recent warming. *Environmental Research Letters,*
915 *15*, 114018.

916 Shim C, Hong J, Hong J, Kim Y, Kang M, Thakuri BM, et al. (2014) Evaluation of MODIS GPP
917 over a complex ecosystem in East Asia: A case study at Gwangneung flux tower in
918 Korea. Advances in Space Research.;54(11):2296–308.

919 Taylor, C.M., Jeu, R.D., Guichard, F., Harris, P.P., & Dorigo, W.A. (2012). Afternoon rain more
920 likely over drier soils. Nature, 489, 423-426.

921 Tjiputra, J., Olsen, A., Assmann, K.M., Pfeil, B., & Heinze, C. (2011). A model study of the
922 seasonal and long-term North Atlantic surface pCO(2) variability. *Biogeosciences, 9*,
923 907-923.

924 Tjiputra, J., Roelandt, C., Bentsen, M., Lawrence, D.M., Lorentzen, T., Schwinger, J., Seland,
925 Ø., & Heinze, C. (2012). Evaluation of the carbon cycle components in the Norwegian
926 Earth System Model (NorESM). *Geoscientific Model Development, 6*, 301-325.

927 Turner, D.P., Ritts, W.D., Cohen, W.B., Gower, S.T., Running, S.W., Zhao, M., Costa, M.H.,
928 Kirschbaum, A., Ham, J.M., Saleska, S.R., & Ahl, D.E. (2006). Evaluation of MODIS

NPP and GPP products across multiple biomes. *Remote Sensing of Environment, 102*, 282-292.

Ulaby, F.T., Moore, M.K., & Fung, A.K. (1982). Microwave Remote Sensing, Active and Passive: Radar Remote Sensing and Surface Scattering and Emission Theory, Vol. 2. Norwood, MA: Artech House

Wagner, W., Hahn, S., Kidd, R., Melzer, T., Bartalis, Z., Hasenauer, S., Figa-Saldana, J., Rosnay, P.D., Jann, A., Schneider, S., Komma, J., Kubu, G., Brugger, K., Aubrecht, C., Züger, J., Gangkofner, U., Kienberger, S., Brocca, L.L., Wang, Y., Blöschl, G., Eitzinger, J., & Steinnocher, K. (2013). The ASCAT Soil Moisture Product: A Review of its Specifications, Validation Results, and Emerging Applications. *Meteorologische Zeitschrift, 22*, 5-33.

Whitaker, J.S., & Hamill, T.M. (2002). Ensemble Data Assimilation without Perturbed Observations. *Monthly Weather Review, 130*, 1913-1924.

Yang, K., Qin, J., Zhao, L., Chen, Y., Tang, W., Han, M., Lazhu, Chen, Z., Lv, N., Ding, B., Wu, H., & Lin, C. (2013). A Multiscale Soil Moisture and Freeze-Thaw Monitoring Network on The Third Pole. *Bulletin of the American Meteorological Society, 94*, 1907-1916.

Zheng, W., Zhan, X., Liu, J., & Ek, M.B. (2018). A Preliminary Assessment of the Impact of Assimilating Satellite Soil Moisture Data Products on NCEP Global Forecast System. Advances in Meteorology.

Zreda, M., Shuttleworth, W.J., Zeng, X., Zweck, C., Desilets, D., Franz, T.E., & Rosolem, R. (2012). COSMOS: the COsmic-ray Soil Moisture Observing System. *Hydrology and Earth System Sciences, 16*, 4079-4099.